Electronic Supplementary Material (ESI) for Journal of Materials Chemistry A.
This journal is © The Royal Society of Chemistry 2019

Electronic Supplementary Information

Single iron atoms stabilized by microporous defects of biomass-derived carbon aerogels as high-performance cathode electrocatalysts for Al-air batteries

Ting He,[a,b] Yaqian Zhang,[c] Yang Chen,[a] Zhenzhu Zhang,[a] Haiyan Wang,[a] Yongfeng Hu,[d] Min Liu,[e] Chih-Wen Pao,[f] Jeng-Lung Chen,[f] Lo Yueh Chang,[g,h] Zhifang Sun,[a,*] Juan Xiang, [a] Yi Zhang[a,*] and Shaowei Chen[b,*]

[a] *Hunan Provincial Key Laboratory of Efficient and Clean Utilization of Manganese Resources, School of Chemistry and Chemical Engineering, Central South University, Changsha 410083 (China), allensune@gmail.com; yzhangcsu@csu.edu.cn*

[b] *Department of Chemistry and Biochemistry, University of California, 1156 High Street, Santa Cruz, California 95064 (United States), shaowei@ucsc.edu*

[c] *Department of Chemical and Materials Engineering, University of Alberta, Edmonton, Alberta T6G 1H9 (Canada)*

[d] *Canadian Light Source, Saskatoon, Saskatchewan (Canada)*

[e] *Institute of Super-Microstructure and Ultrafast Process in Advanced Materials, School of Physics and Electronics, Central South University, Changsha 410083 (China)*

[f] *X-ray Absorption Group, National Synchrotron Radiation Research Center, Hsinchu 30076 (Taiwan, Republic of China)*

[g] *Institute of Functional Nano & Soft Materials (FUNSOM), Soochow University, Suzhou, Jiangsu 215123 (China)*

[h] *Soochow University- Western University Centre for Synchrotron Radiation Research, Suzhou, Jiangsu 215123 (China)*

Table S1 Elemental contents of the various catalysts determined by XPS.

elements	CA_{LR} at %	NCA_{LR} at %	CA_{LR}/Fe at %	NCA_{LR}/Fe at %
C	97.85	94.43	95.49	94.86
O	2.09	2.30	2.18	2.07
N	0.06	3.27	2.21	2.74
Fe	0	0	0.12	0.34

Table S2 EDS data for the NCA_{LR}/Fe catalyst

elements	wt %	at %
C	90.10	92.30
N	5.40	04.80
O	3.50	02.70
Fe	0.90	0.20

Table S3 Iron contents of the various catalysts determined by ICP-OES

Sample	Concentration (mg/L)	Mass of Fe (mg)	Total mass (mg)	wt%
NCA_{LR}	0.00	0	2.8	0.000
CA_{LR}/Fe	0.018	0.0018	3.2	0.056
NCA_{LR}/Fe	0.32	0.032	2.4	1.33

Table S4 BET surface area and pore distribution of the CA_{LR}, NCA_{LR}, CA_{LR}/Fe and NCA_{LR}/Fe catalysts.

Sample	S_{BET} (m^2 g^{-1})	Pore volumes (cm^3 g^{-1})	Pore volume percentage (%)		
			micropore	mesopore	macropore
CA_{LR}	857.3	1.306	19.8	77.1	3.1
NCA_{LR}	719.3	0.75	36.1	60.5	3.3
CA_{LR}/Fe	777.2	1.12	23.4	71.1	5.5
NCA_{LR}/Fe	699.8	0.91	24.2	71.0	4.8

Table S5 EXAFS fitting results of NCA_{LR}/Fe by using FePc as a reference.

Sample	N	R	σ^2
NCA_{LR}/Fe	4	1.96960	0.00724
FePc	4	1.97578	0.01088

Table S6 Comparison of the ORR performance of the NCA_{ST}/Fe catalyst with results of relevant TM−N/C catalysts in recent literatures

Materials	Half-wave potential (V)	Ref.
NiCo alloy/carbon nanofibers	0.80	[1]
Co nanoparticles/3D Carbon	0.83	[2]
Carbon nanosphere/single-atom catalysts	0.84	[3]
Bimetal/nitrogen co-doped carbon	0.85	[4]
Copper single atom catalyst	0.87	[5]
Single cobalt atoms catalyst	0.88	[6]
Single-atom $Fe\text{-}N_4$ catalyst	0.88	[7]
Biomass hydrogel derived single Fe atom	0.88	This work
Single Fe atoms/N-doped carbon	0.90	[8]

Table S7 Electron transfer numbers (n) for different catalysts.

Potential	NCA_{LR}/Fe	CA_{LR}/Fe	NCA_{LR}	CA_{LR}
0.8	3.85	2.83	3.27	2.84
0.7	3.83	2.56	3.62	2.91
0.6	3.85	2.31	3.26	2.41
0.5	3.87	2.47	3.31	2.51
0.4	3.92	2.82	3.45	2.75
0.3	3.96	3.26	3.57	3.08
0.2	4.00	3.55	3.73	3.39
Average n	3.90	2.83	3.46	2.84

Table S8 Electron transfer numbers (n) for the NCA_{LR}/Fe catalyst in the acidic medium.

Potential (V)	0.7	0.6	0.5	0.4	0.3	0.2	Average N
n	3.88	3.6	3.75	3.84	3.87	3.97	3.82

Table S9 Al-air battery performance of this work and other literatures.

Catalysts	Maximal power density/ mW cm^{-2}	Open circuit voltage/ V	Voltage at 20 mA cm^{-2}/V
This work	**181.1**	**1.81**	**1.70**
Commercial Pt/C	175.0	1.79	1.64
Co-doped carbon[9]	161.1	1.70	
Fe/N co-doped carbon[10]			1.68
Cu/Fe-N-C[11]			1.64
Fe_3C@Fe/N-G-1[12]	129.9		1.56
Fe-Co/N-doped C[13]			1.46
Defect-engineered MnO_2[14]	159	1.90	

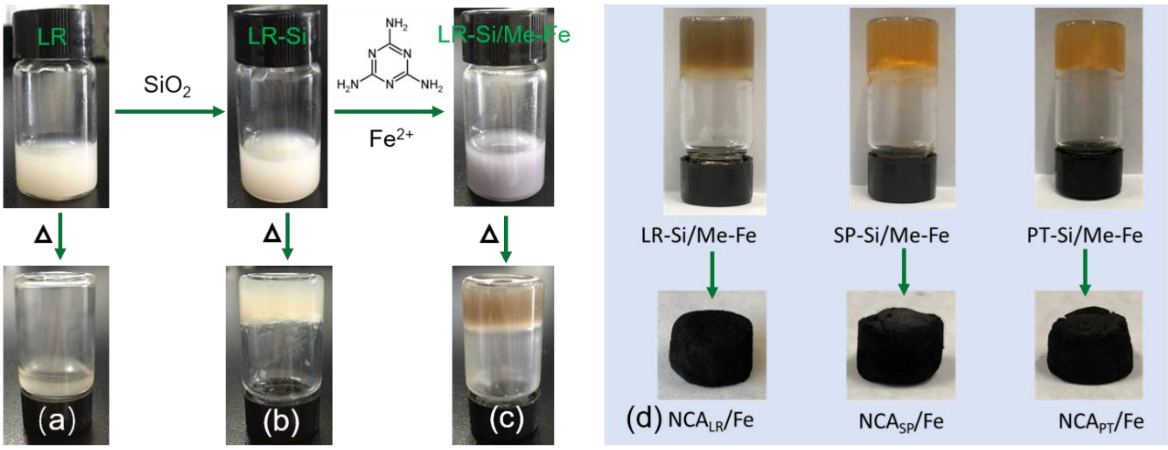

Fig. S1 Digital photographs of LR sol and hydrogels: (a) LR sol, (b) LR-Si hydrogel, and (c) LR-Si/Me-Fe hydrogels. (d) Biomass hydrogels that are used to synthesize carbon aerogels embedded with single Fe atom catalysts.

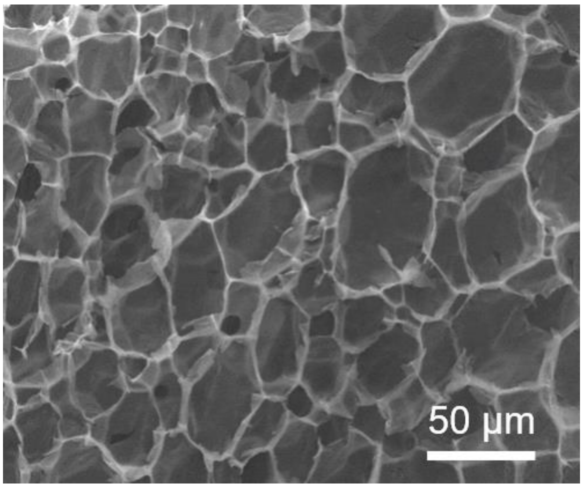

Fig. S2 SEM image of LR hydrogel.

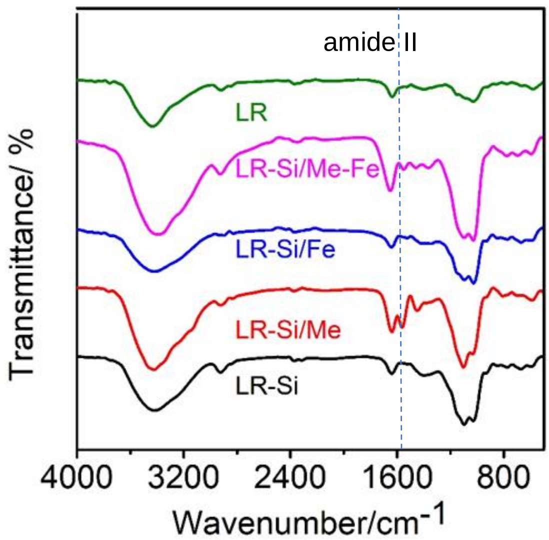

Fig. S3 FTIR spectra of LR-Si, LR-Si/Me, LR-Si/Fe, LR-Si/Me-Fe and LR hydrogels.

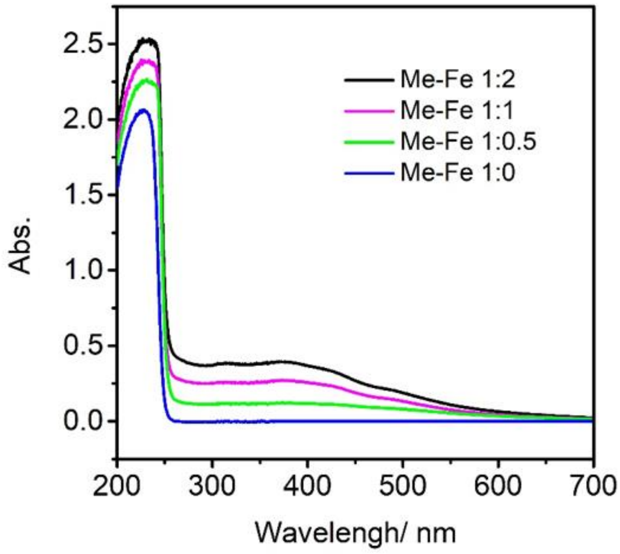

Fig. S4 UV-vis spectra of the Me-Fe complex at different melamine:Fe ratios. At increasing Fe loading, the major absorption peak of the melamine-Fe sol (215 nm) becomes intensified and red-shifts significantly. In addition, two new peaks appear at 305 nm and 380 nm and grow gradually.

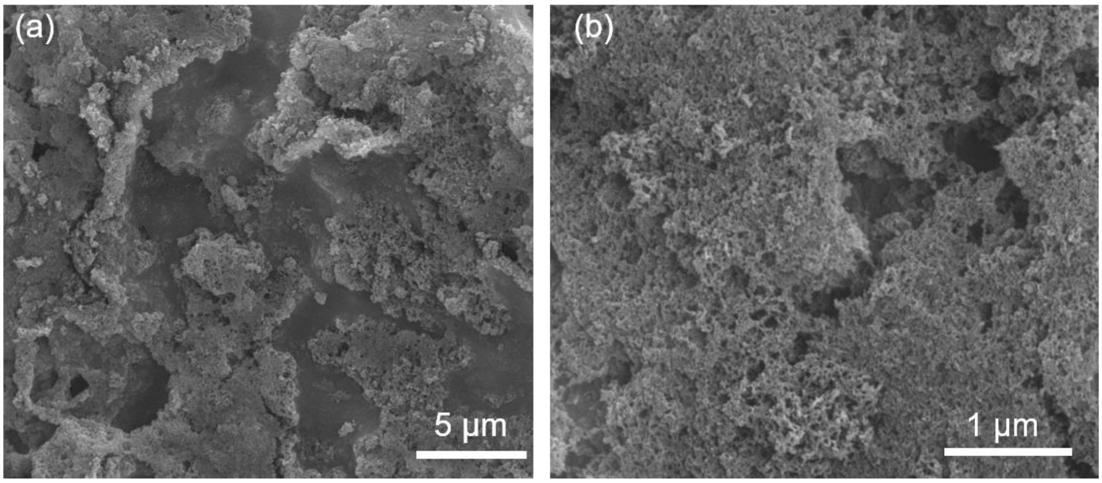

Fig. S5 SEM images of NCA_{LR}/Fe.

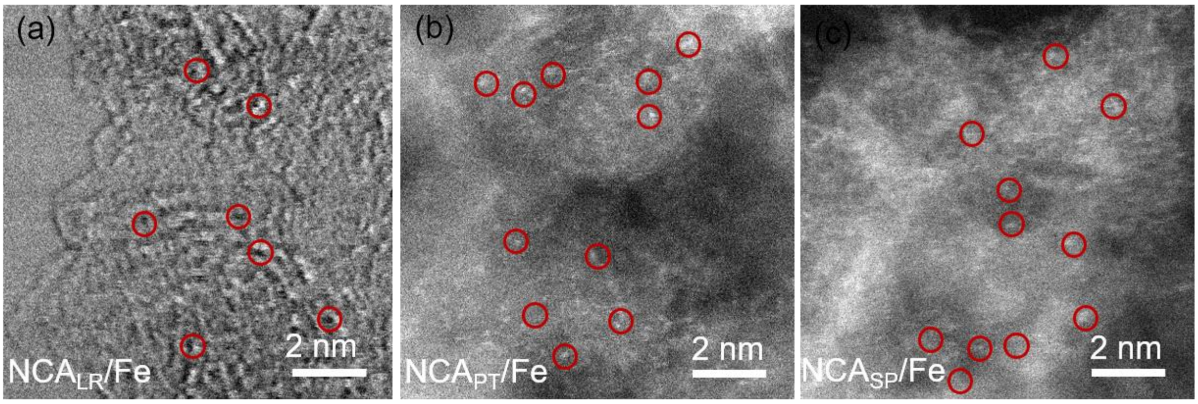

Fig. S6 STEM images of NCA_{LR}/Fe (HAABF), NCA_{PT}/Fe (HAADF) and NCA_{SP}/Fe (HAADF).

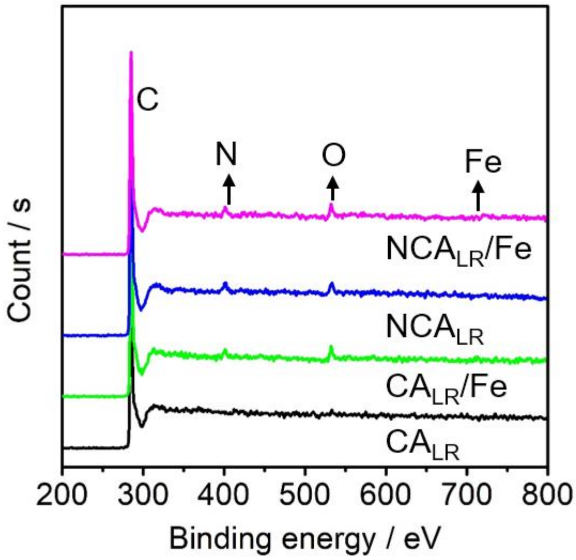

Fig. S7 XPS survey spectra of the CA_{LR}, NCA_{LR}, CA_{LR}/Fe and NCA_{LR}/Fe catalysts.

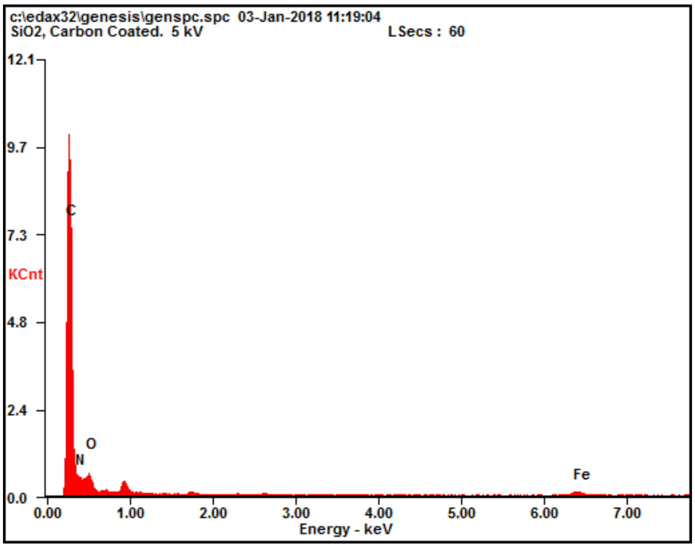

Fig. S8 EDS analysis of the NCA_{LR}/Fe catalyst.

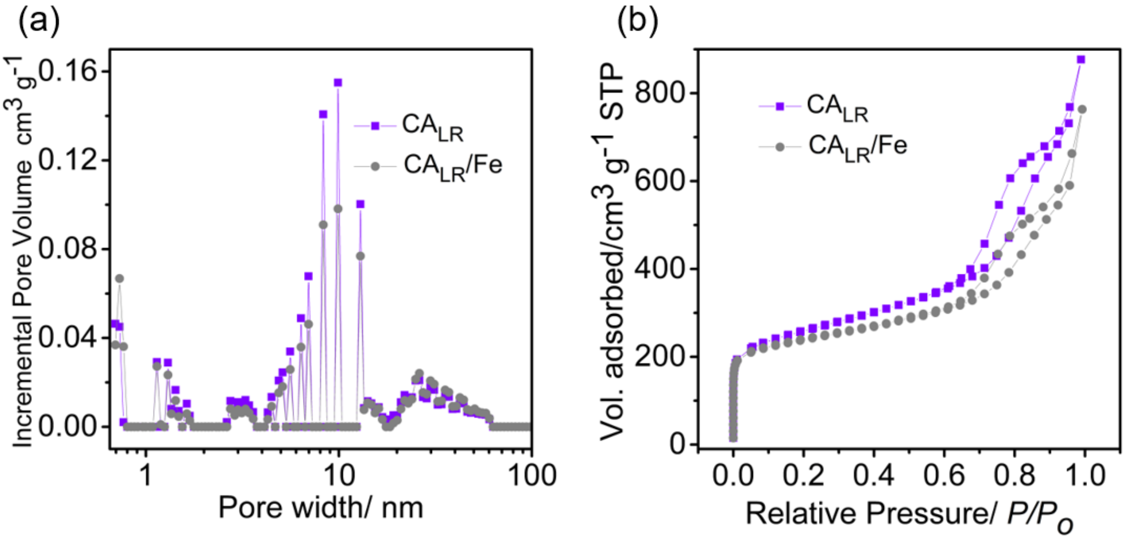

Fig. S9 (a and b) N_2 adsorption-desorption isotherms and (c and d) pore size distribution of the CA_{LR}, NCA_{LR}, CA_{LR}/Fe and NCA_{LR}/Fe catalysts.

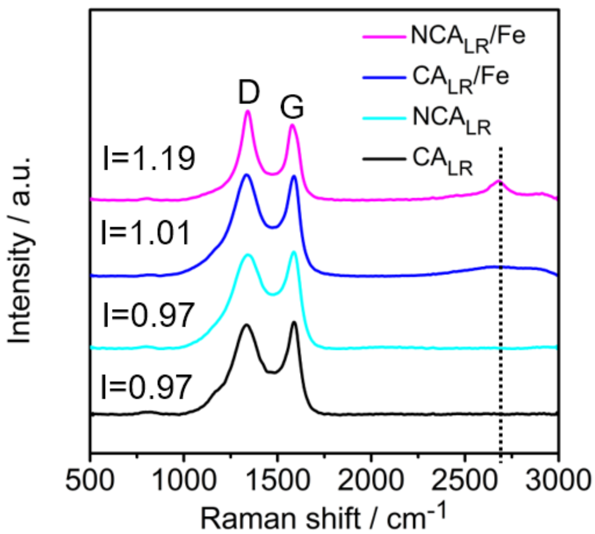

Fig. S10 Raman spectra of the catalysts: CA_{LR}, NCA_{LR}, CA_{LR}/Fe and NCA_{LR}/Fe.

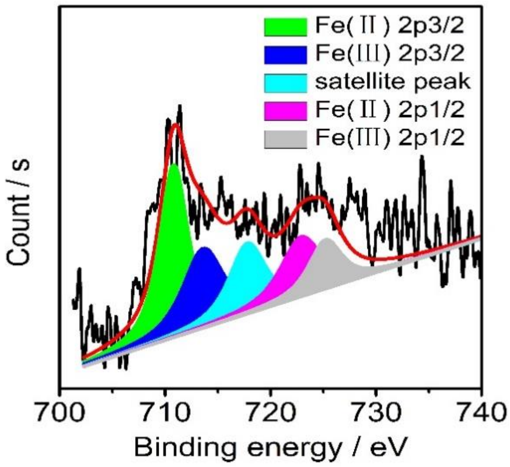

Fig. S11 High-resolution XPS scan of the Fe 2P electrons of NCA_{LR}/Fe.

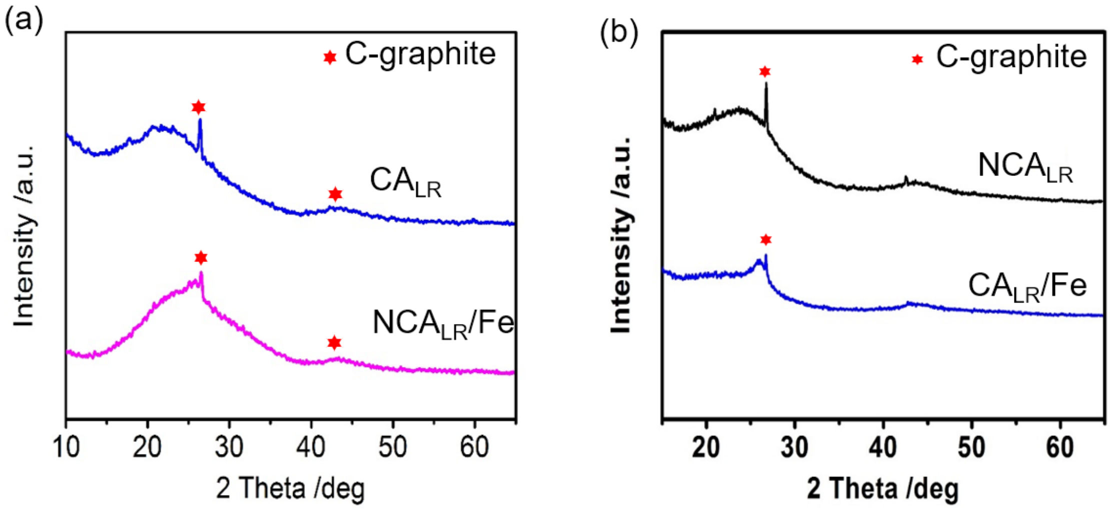

Fig. S12 XRD patterns of the CA_{LR}, NCA_{LR}, CA_{LR}/Fe and NCA_{LR}/Fe catalysts.

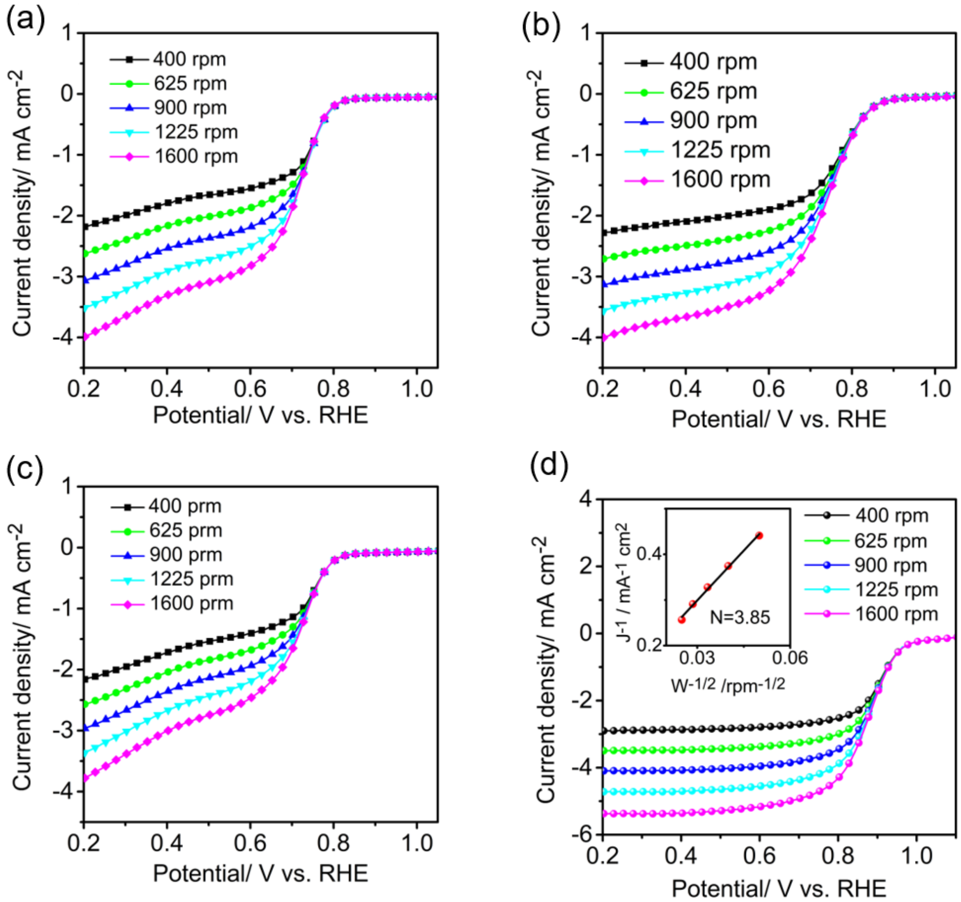

Fig. S13 LSV curves for (a) CA_{LR}, (b) NCA_{LR}, (c) CA_{LR}/Fe and (d) NCA_{LR}/Fe at different rotation rates in 0.1 M KOH, inset to panel (d) is the Koutecky-Levich plot at +0.85 V.

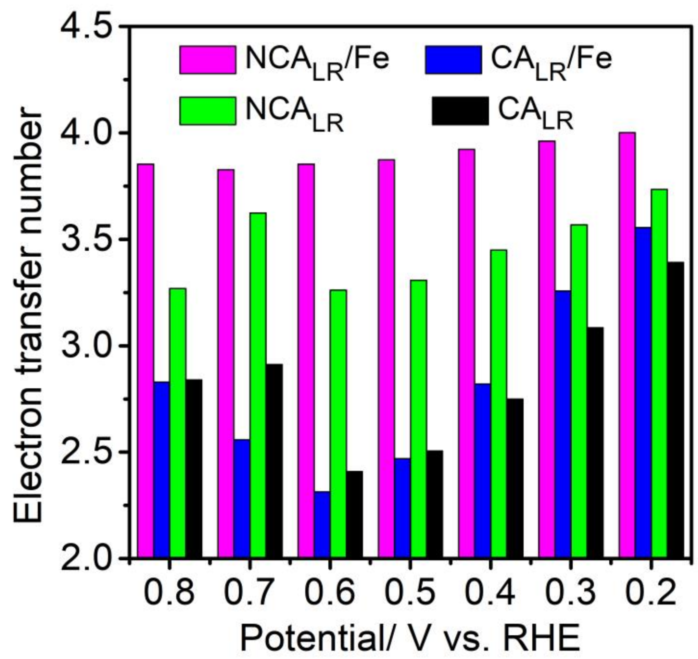

Fig. S14 Electron transfer numbers of various catalysts at different potentials.

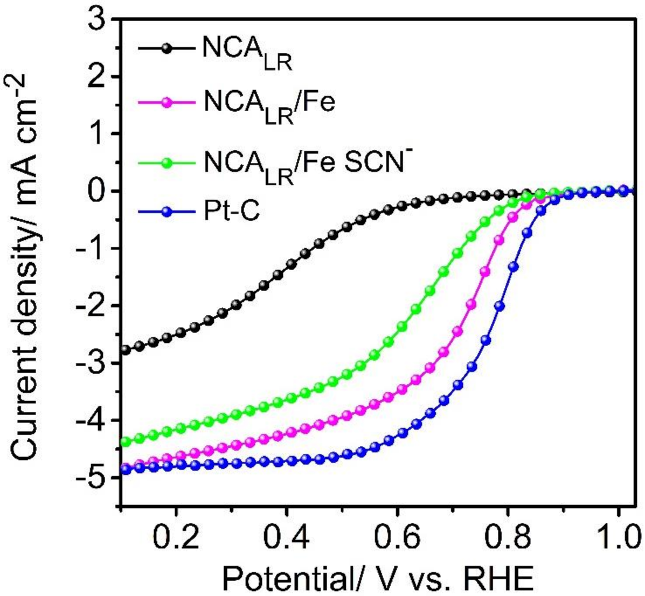

Fig. S15 LSVs of NCA$_{LR}$, NCA$_{LR}$/Fe (without or with 10 mM SCN$^-$) and Pt/C as ORR catalysts at 1600 rpm; scan rate: 5 mV s^{-1}, medium: O_2-saturated 0.1 M $HClO_4$.

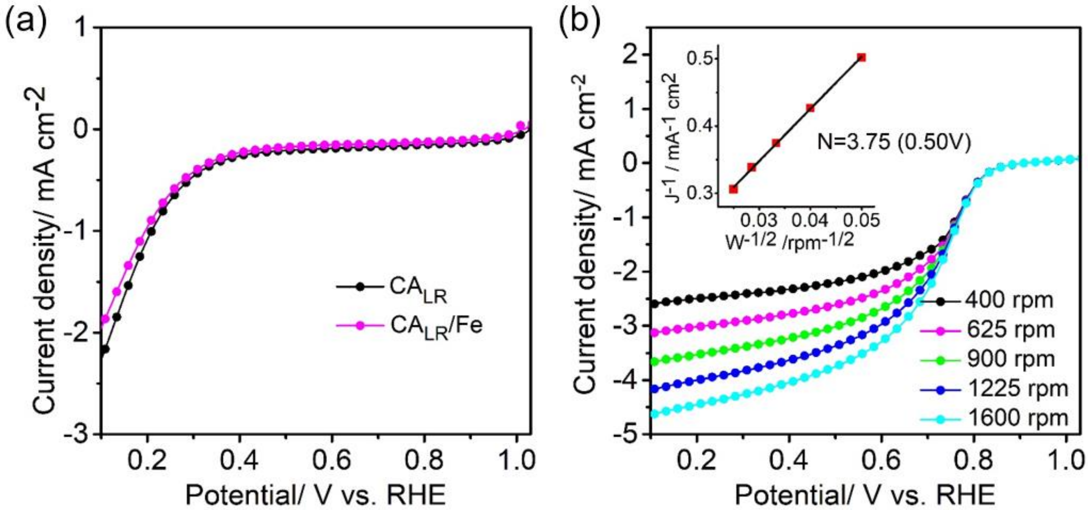

Fig. S16 (a) LSVs of the CA$_{LR}$ and CA$_{LR}$/Fe in O_2-saturated 0.1 M $HClO_4$. (b) LSVs of the NCA$_{LR}$/Fe at different rotation rates. Inset to panel (b) is the Koutecky-Levich plot at 0.50 V. Scan rate 5 mV s^{-1}.

The ORR activity in acidic medium (0.1 M $HClO_4$) was also investigated. As shown in Fig. S9 and S10, the NCA$_{LR}$/Fe sample exhibits a half-wave potential of +0.72 V, which is very close to that of Pt/C (+0.77 V). Table S3 lists the average n value (3.82) of the NCA$_{LR}$/Fe within the potential range of +0.2 V to +0.7 V, again, suggesting a 4e$^-$ reaction pathway from O_2 to H_2O. To explore the function of single metal atom sites in the NCA$_{LR}$/Fe catalyst, SCN$^-$ was added during the tests as they could strongly coordinate with the metal sites. As shown in Fig. S9 and S11, upon the addition of SCN$^-$ into the acidic medium, the $E_{1/2}$ of the NCA$_{LR}$/Fe catalyst shifts negatively by ca. 90 mV, suggesting that the ORR activity is dominated by the Fe atom sites.

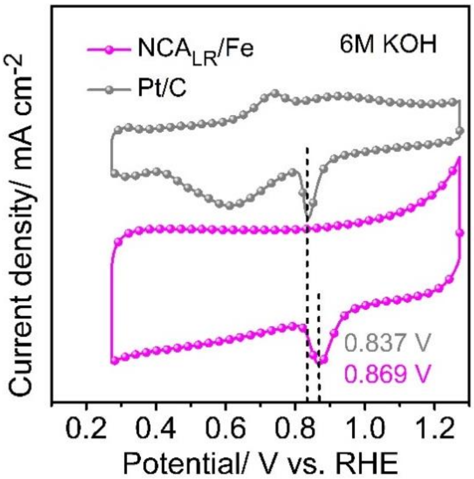

Fig. S17 CV of NCA_{LR}/Fe and Pt/C as ORR catalysts in 6 M KOH.

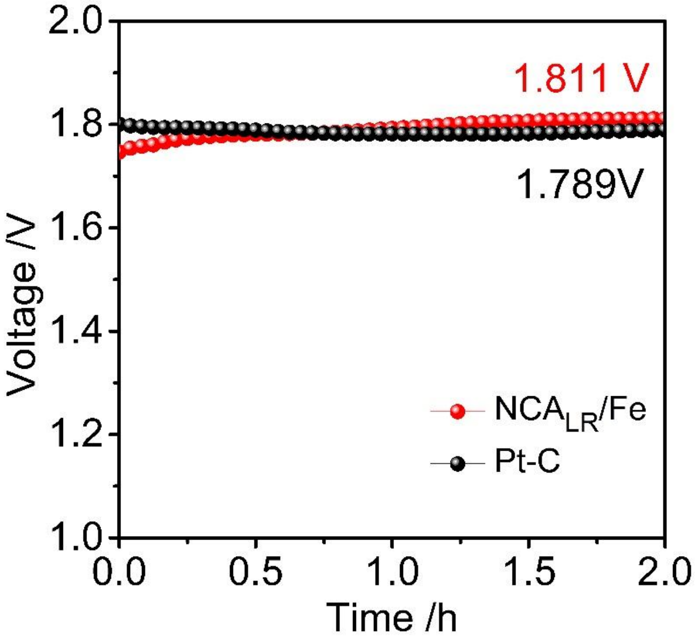

Fig. S18 Open circuit voltage tests of NCA_{LR}/Fe and Pt/C.

Supplementary References

[1] Y. Fu, H.-Y. Yu, C. Jiang, T.-H. Zhang, R. Zhan, X. Li, J.-F. Li, J.-H. Tian, R. Yang, *Adv. Funct. Mater.* **2018**, *28*, 1705094.
[2] H. Jiang, Y. Liu, W. Z. Li, J. Li, *Small* **2018**, *14*.
[3] A. Han, W. Chen, S. Zhang, M. Zhang, Y. Han, J. Zhang, S. Ji, L. Zheng, Y. Wang, L. Gu, C. Chen, Q. Peng, D. Wang, Y. Li, *Adv. Mater.* **2018**, *30*, e1706508.
[4] M. L. Tan, T. He, J. Liu, H. Q. Wu, Q. Li, J. Zheng, Y. Wang, Z. F. Sun, S. Y. Wang, Y. Zhang, *Journal of Materials Chemistry A* **2018**, *6*, 8227.
[5] F. Li, G.-F. Han, H.-J. Noh, S.-J. Kim, Y. Lu, H. Y. Jeong, Z. Fu, J.-B. Baek, *Energy Environ. Sci.* **2018**.
[6] P. Yin, T. Yao, Y. Wu, L. Zheng, Y. Lin, W. Liu, H. Ju, J. Zhu, X. Hong, Z. Deng, G. Zhou, S. Wei, Y. Li, *Angew. Chem. Int. Ed.* **2016**, *55*, 10800.
[7] Y. Pan, S. Liu, K. Sun, X. Chen, B. Wang, K. Wu, X. Cao, W. C. Cheong, R. Shen, A. Han, Z. Chen, L. Zheng, J. Luo, Y. Lin, Y. Liu, D. Wang, Q. Peng, Q. Zhang, C. Chen, Y. Li, *Angew. Chem. Int. Ed.* **2018**, *57*, 8614.
[8] Y. Chen, S. Ji, Y. Wang, J. Dong, W. Chen, Z. Li, R. Shen, L. Zheng, Z. Zhuang, D. Wang, Y. Li, *Angew. Chem. Int. Ed.* **2017**, *56*, 6937.
[9] J. Li, Z. Zhou, K. Liu, F. Li, Z. Peng, Y. Tang, H. Wang, *J. Power Sources* **2017**, *343*, 30.
[10] J. Li, J. Chen, H. Wang, Y. Ren, K. Liu, Y. Tang, M. Shao, *Energy Storage Materials* **2017**, *8*, 49.
[11] J. Li, J. Chen, H. Wan, J. Xiao, Y. Tang, M. Liu, H. Wang, *Applied Catalysis B: Environmental* **2019**, *242*, 209.
[12] K. Liu, Z. G. Peng, H. Y. Wang, Y. R. Ren, D. P. Liu, J. S. Li, Y. G. Tang, N. Zhang, *Journal of the Electrochemical Society* **2017**, *164*, F475.
[13] M. Tan, T. He, J. Liu, H. Wu, Q. Li, J. Zheng, Y. Wang, Z. Sun, S. Wang, Y. Zhang, *Journal of Materials Chemistry A* **2018**, *6*, 8227.
[14] M. Jiang, C. Fu, J. Yang, Q. Liu, J. Zhang, B. Sun, *Energy Storage Materials* **2019**, *18*, 34.